Flux-flow voltages during guided flux collapse from hollow superconducting cylinders*

S. M. Khanna†
Space Sciences Laboratory, ES24 NASA, Marshall Space Flight Center, Alabama 35812

John R. Clem‡
Ames Laboratory-ERDA and Department of Physics, Iowa State University, Ames, Iowa 50010

M. A. R. LeBlanc
Physics Department, University of Ottawa, Ottawa, Canada K1N 9B4
(Received 9 October 1975)

Voltages across diametrically opposite contact pairs on the outer surface of superconducting Nb tubes are found to depend dramatically upon the spatial configuration of the voltage measuring leads relative to the positions of the moving magnetic flux lines. Experiments have been conducted to study these voltages for different wall thicknesses and for a variety of arrangements of the leads when flux in the hole and the wall of the Nb tube is made to exit or enter, completely or partially, by applying heat at a narrow strip along its length. The basic concepts of the origin of flux-flow voltages in superconductors are discussed and the importance of the measuring-circuit configuration is stressed. Using the critical-state concept, a model for the change of flux and the resulting electric fields in the Nb tube on application of a heat pulse is presented. The resulting time-dependent and time-integrated voltages are calculated and are in excellent quantitative agreement with our present experimental results. These results show that the flux-flow voltages across two contact points on a superconductor arise from (i) the generation of an induced electric field over a chosen path in the superconductor between the contact points and (ii) a change of magnetic flux through the surface bounded by the measuring leads and the chosen path in the superconductor. Furthermore, the movement of vortex-line segments deep within the superconductor makes no contribution to the measured signal. Use of the flux-flow signals in the study of the dynamics of vortex motion during flux jumps in hollow superconducting tubes is discussed.

I. INTRODUCTION

It is well established that the flux-flow voltages in the mixed states of a type-II superconductor under steady conditions of applied magnetic field, transport current, and/or temperature gradient are produced by the motion of vortices (flux quanta).[1,2] Some questions remain, however, regarding the precise nature of the time-dependent flux-flow voltage detected by a conventional voltmeter connected by leads to the specimen's surface, especially when the vortex array is inhomogeneous and moves with a time-dependent velocity.[3-8] One question, for example, is to what extent the voltage depends upon the spatial configuration of the measuring-circuit leads. Such a dependence has been observed in flux-flow voltage-noise experiments,[8] in thermally induced flux-collapse measurements,[6] and in several other experiments.[9] Another question is whether vortex-line segments moving deep within the superconductor contribute to the measured voltage.

In this paper, we describe results of an experiment which help to answer these questions. Essentially, the experiment shows that a specified change of magnetic flux in a hollow superconductor, which is part of a fixed measuring circuit, produces a voltage, measured across two contact points on the superconductor, that is dramatically dependent on the spatial configuration of the voltage measuring leads. Moreover, our results are consistent with the statement that a conventional voltmeter, connected to contacts on the surface of a superconductor, is insensitive to the motion of vortex-line segments deep within the superconductor and that the measured voltage is produced primarily by vortex-line segments moving within a few penetration depths of the surface. All our results can be explained theoretically if we express the measured voltage as the sum of two terms: a line integral of the effective electric field along a path in the superconductor between the two contacts, and the time rate of change of magnetic flux through the surface bounded by this path and the measuring-circuit leads.

In Sec. II, we discuss in general the flux-flow voltages measured by a conventional voltmeter across two contact points on the surface of a superconductor. The experimental procedure and results for the flux-flow voltages across a hollow superconducting cylinder when the flux trapped in the cylinder is changed under different conditions are described in Secs. III and IV. In Sec. V, we calculate the flux-flow voltages across the contact points on the surface of a hollow superconducting cylinder for the conditions of the present experi-

ment. Our experimental results are compared with the calculations in Sec. VI. Our results are summarized in Sec. VII.

A brief description of some of the present results has been reported earlier by two of the authors (S.M.K. and M.A.R.L.).[10] Although the discussion given in that paper provides for a simple and essentially correct explanation of the present results, it is not complete as it does not give the total dynamical picture of collapse of flux in the cylinder described in the present paper.

II. FLUX-FLOW VOLTAGES IN SUPERCONDUCTORS

The measured flux-flow voltage between any two points a and b on the surface of a superconductor is given by[5] (Fig. 1)

$$V_{ab} = V_A - V_B = \int_{a[C_L]}^{b} \vec{E}' \cdot d\vec{l} - \frac{1}{c}\frac{d}{dt}\Phi_{ML} \quad . \qquad (2.1)$$

Here, the effective electric field[1] $\vec{E}' = (m/e)\nabla\mu - (1/c)(d\vec{A}/dt)$ is the gauge-invariant generalization of the gradient of the chemical potential μ; m and $-e$ are the electronic mass and charge; $\vec{A}$ is the vector potential; $\vec{B} = \nabla \times \vec{A}$ is the magnetic flux density or magnetic induction; C_L is any path from a to b in the superconductor; and

$$\Phi_{ML} = \int_{[S_{ML}]} \vec{B} \cdot \hat{n}\, dS \qquad (2.2)$$

is the magnetic flux through the surface S_{ML} bounded by paths C_M and C_L in the direction of unit normal $\hat{n}$ shown in Fig. 1.

Quite generally, the first term on the right-hand side of Eq. (2.1) represents the voltage contribution from an electric field over the path C_L through the superconductor and the second term represents the induced emf from the change of flux in the closed loop bounded by the paths C_L and C_M. The voltage V_{ab} is independent of the choice of path C_L, since $\vec{E}'$ and $\vec{B}$ obey Faraday's law, $\nabla \times \vec{E}' = (-1/c)(d\vec{B}/dt)$, and thus any change in the first term on the right-hand side of Eq. (2.1) along an alternative path is completely canceled by an equivalent change in its second term. V_{ab}, of course, depends on the position of the contact points a and b and on the choice of the area S_{ML} and, hence, upon the fixed position of the measuring-circuit leads constituting the contour C_M.

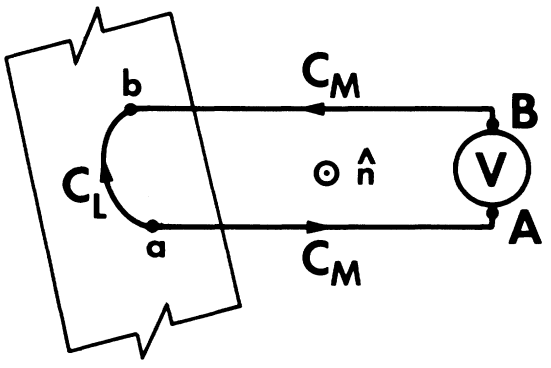

FIG. 1. Schematic view of voltage measuring circuit attached at two points a and b on the superconductor surface.

The role of the contribution $(-1/c)(d\Phi_{ML}/dt)$ to flux-flow voltages should be understood clearly. As mentioned above, $\vec{E}'$ and $\vec{B}$ are related by Faraday's law and thus the induced voltage due to flux changes in the superconductor alone may be incorporated in either of the two terms on right-hand side of Eq. (2.1) by the appropriate choice of path C_L. In addition to this, Φ_{ML} also includes the external flux outside the superconductor through the surface bounded by the measuring leads and the specimen's surface. This has been shown to be important in some measurements.[6,8] Although the time average of this external contribution to the term $(-1/c)(d\Phi_{ML}/dt)$ is zero in typical flux-flow measurements, its instantaneous value is not, in general, zero and is important in some cases, such as in flux-flow voltage-noise measurements.

The origin of the measured flux-flow voltages during vortex motion through the superconductor has long been a subject of discussion.[1-6] We believe that these voltages are properly described as follows: The observed flux-flow voltage at any given time is, in general, a linear superposition of voltage pulses produced by all vortices moving in the superconductor. The magnitude of the time *integral* of the voltage pulse produced by a single vortex can be shown to be $\phi_0/c = h/2e$ multiplied by the number of times the vortex axis passes between the contacts during its lifetime. To estimate the *time* dependence of the pulse produced by a given vortex moving through a specimen whose dimensions are large by comparison with the penetration depth, we must make two observations. First, the magnetic flux ϕ_0 carried through the interior of the superconductor along the vortex axis passes into the space near the superconductor and returns around the specimen. The time dependence of the fraction of the return flux that passes through the measuring circuit makes an important contribution to the observed voltage pulse. This contribution depends upon the spatial configuration of the measuring-circuit leads. Second, the moving vortex produces a contribution to the electric field that is localized in the

vicinity of the vortex core and near the surface of the superconductor, and which decays approximately exponentially within a few (field-dependent) penetration depths from the core or the surface. In general, the contributions from a given vortex to *both* $\vec{B}$ and E' must be substituted into Eq. (2.1) to obtain the corresponding net contribution to V_{ab}. As shown in Refs. 3 and 5, for the computation of a voltage pulse it is most convenient to choose C_L to lie for most of its length more than a few penetration depths from both the specimen's surface and the axis of the moving vortex line producing the pulse.

To illustrate the use of this procedure, we consider the motion of a single vortex, moving with a constant velocity across a superconducting slab in the presence of an applied magnetic field directed as shown in Fig. 2. According to the principle of superposition, we can ignore the applied field, concentrate on the contribution from the vortex alone, and use Eq. (2.1) to determine the voltage signals in different cases [(a)–(d)]. We choose the path C_L (shown dashed) to avoid the surface and the vortex core, such that the entire contribution to the voltage pulse is represented by the last term in Eq. (2.1), $-c^{-1}d\Phi_{ML}/dt$. For the measuring-circuit configuration of Fig. 2(a), the net flux Φ_{ML} through the shaded area S_{ML} decreases monotonically from ϕ_0, when the vortex is near the left side, to zero when the vortex is at the right side. The resulting voltage pulse is rather large at all times during the transit of the vortex across the specimen. For the circuits of Figs. 2(b)–2(d), however, in which the leads are kept close either to the specimen's surface or to each other, the flux Φ_{ML} changes rapidly from ϕ_0 to zero during the time that the vortex passes under the segments *bc* in Figs. 2(b) and 2(d) or under the segment *cd* in Fig. 2(c).

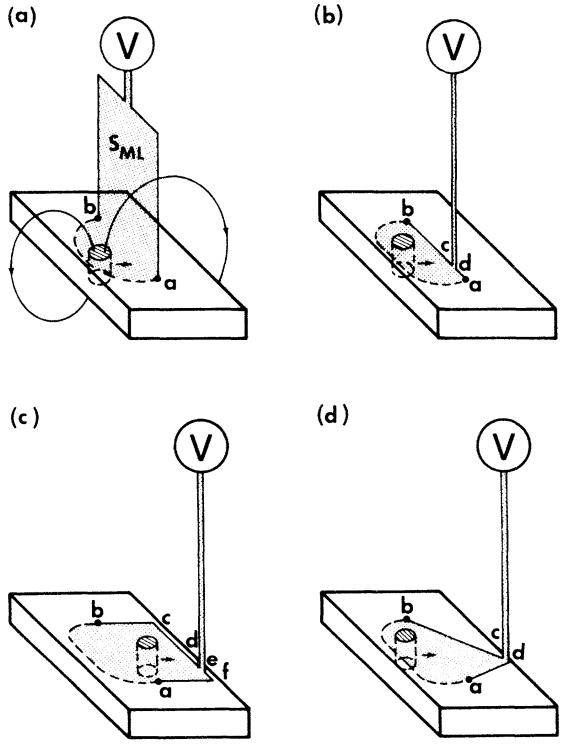

FIG. 2. As described in the text, the flux-flow voltage $V_{ab}(t)$ depends upon the different possible orientations (a), (b), (c), and (d) of the voltage measuring leads relative to the direction of magnetic induction and motion of a vortex line in the superconductor. The time-*integrated* voltage, however, corresponds to the flux in the vortex and is the same in all cases. (The size of the vortex is here greatly exaggerated for clarity.)

Thus, for the case of a single vortex and, by superposition, for the case of an inhomogeneous array of vortices, the measured instantaneous flux-flow voltage depends upon the position of the contact points on the superconductor, the spatial configuration of the measuring-circuit leads relative to the surface, and the position, speed, and direction of motion of the moving vortices in the superconductor. *In the special case for which the measuring-circuit leads are kept close either to the specimen's surface or to each other, such that there is no open area bounded by the leads and the surface, the instantaneous measured voltage is produced only by those vortices that are being created, moving, or annihilating in the immediate vicinity of the leads lying along the surface of the superconductor.*

For a moving array of vortices it is sometimes more convenient to obtain the electric field $\vec{E}'$ from[1,2]

$$\vec{E}' = \vec{B} \times \vec{v}/c \tag{2.3}$$

and to evaluate the line integral in Eq. (2.1) directly. Here, $\vec{E}'$ and $\vec{B}$ are averages over several intervortex spacings, and $\vec{v}$ is the local vortex velocity which is perpendicular to $\vec{B}$ by definition; that is, we consider spatial variations of $\vec{E}'$ and $\vec{B}$ on the scale of the specimen dimensions and ignore variations on the scale of the intervortex spacing.

In the normal state, the electric field becomes

$$\vec{E}' = \vec{E}'_n = \rho_n \vec{J}_n = (c\rho_n/4\pi)\,\nabla \times \vec{H}, \tag{2.4}$$

where ρ_n is the normal-state resistivity, $\vec{J}_n$ is the current density, and $\vec{H}$ ($=\vec{B}$) is the local magnetic field.

III. EXPERIMENTAL PROCEDURE

Two hollow cylinders of niobium, identical in length and inner diameter, but differing in wall thickness, were studied (Fig. 3). Their dimen-

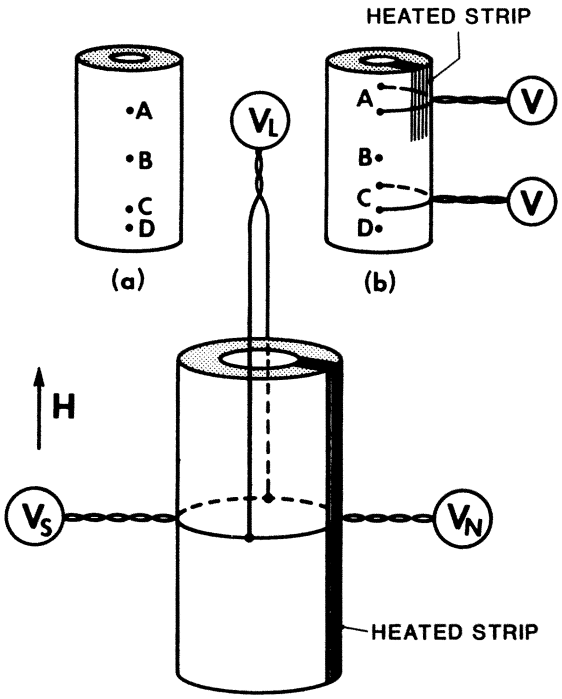

FIG. 3. Schematic view of experimental arrangement. The pick up coils, central heater, and one of the strip heaters are not shown for clarity. Inset (a) shows the location of the pairs of contact points along the length of the cylinder. Inset (b) shows the voltage measuring circuits when a hair-pin heater is used to heat only a part of the length of the specimen.

sions were 2.77-cm i.d., 7.62-cm length, and (i) 0.203-cm wall thickness for sample 1 and (ii) 0.064-cm wall thickness for sample 2. Two heater coils (strip heaters) placed diametrically opposite to one another were wound longitudinally and were in intimate thermal contact with the inner and outer surfaces of the wall of the cylinder along its entire length and over a strip $\simeq 0.5$ cm wide. Another heater coil (central heater) was placed inside the Nb tube and was in intimate thermal contact with its entire inner surface. All of these heater coils were noninductively (bifilar) close-wound single-layer coils of 0.010-cm-diam Formvar insulated manganin wire.

Several pairs of voltage contacts were made at the outer surface of the cylinder. For each pair, voltage contacts were made at two diametrically opposite points halfway between the strip heaters. Three pairs of measuring leads held close to the outer surface of the cylinder were brought out from each pair of voltage contacts, one pair of leads toward each of the strip heaters and the third pair along the length of the cylinder as shown in Fig. 3. The pairs of voltage contacts were positioned at the following distances from the top end of the cylinder along its length L: (i) $0.5L$ and (ii) $0.75L$ in sample 1; (i) $0.2L$, (ii) $0.5L$, (iii) $0.75L$, and (iv) $0.8L$ in sample 2 [Fig. 3, inset (a)]. A pickup coil (outer coil) of 25 turns of 46 B&S copper wire was wound around the Nb tube at each location of the voltage contacts. Another pickup coil (inner coil) of 100 turns of 46 B&S copper wire and having an inner diameter of 2.72 cm was placed inside the cylinder. The assembly of the Nb cylinder, heaters, and pickup coils was rigidly positioned in the center of a superconducting solenoid of 15-cm length, 3.5-cm i.d., and 4.5-cm o.d., immersed in a helium bath. The solenoid provided a uniform magnetic field along the axis of the Nb cylinder. An electronic pulse circuit with a rise time of a few microseconds provided 0–500-V dc voltage pulses to heaters of duration adjustable from 1 to 2000 msec. This enabled us to heat a narrow strip of the sample wall along its entire length above its transition temperature at a fast rate.

The sample was heated via the central heater and then allowed to cool through T_c to the ambient temperature (4.2°K) in the presence of a stationary externally applied magnetic field H_a. The applied field was then changed slowly to a new value H_f (which may be zero), thereby generating a magnetic moment in the sample. The evolution of this magnetic moment could be continuously monitored against H. In particular, it was essential to ensure that no flux jumps occurred as the applied magnetic field was varied. With the applied field maintained at H_f, the sample was then heated above T_c at a fast rate by applying a suitable voltage pulse to one of the strip heaters. We simultaneously measured the resulting signals across one of the outer pickup coils and the voltage contacts at that location with one of the three configurations of the voltage measuring leads (see Fig. 3). Similar measurements were repeated for all pairs of voltage contacts. We studied the integrated as well as the instantaneous signals across the voltage contacts and the pickup coils by using electronic integrators and a double-beam oscilloscope, respectively. These measurements were calibrated assuming that the sample in the virgin state shielded itself perfectly against entry of a weak field $H \ll H_{c1}$ applied from zero.

Similar measurements were also taken when the sample was placed in a nonuniform field. For this purpose, the sample was positioned coaxially at one end of the solenoid such that half the length of the hollow cylinder was inside and the other half was outside the solenoid. This enabled us to generate strongly varying magnetizations along the length of the cylinder. Flux-flow voltages across a pair of voltage contacts were also investigated

with a special arrangement of voltage measuring leads (see Sec. IV).

For another separate set of measurements, a flat U-shaped, 0.5-cm-wide and 3.0-cm-long (cf. length of cylinder, which is 7.62 cm) bifilar heater (hairpin heater) was placed in intimate thermal contact with the inner and outer surfaces of sample 2 over a strip 0.5 cm wide and 3.0 cm long along the length and placed halfway between the voltage contacts near one end of the cylinder [Fig. 3, inset (b)]. From measurements of signals across the voltage contacts and corresponding pickup coils, this heater enabled us to study the collapse of magnetization in different regions along the length of the sample when only a part of its length was heated to the normal state.

Simultaneous measurements of induced voltages across various pairs of voltage contacts at different positions along the length of the specimen during spontaneous flux jumps as the external field was swept over $0 \rightarrow H_{c2} \rightarrow 0$ were carried out extensively for a variety of conditions. The signals across corresponding pickup coils were also measured simultaneously with the above signals.

IV. RESULTS

We denote the instantaneous and integrated signals observed across a pair of voltage contacts on the Nb tube over a given cross section by V_N and $S_N = \int V_N(t)\,dt$, respectively, when the measuring leads are brought out toward the strip heater used to quench the superconductivity; by V_S and $S_S = \int V_S(t)\,dt$, respectively, when they are taken out away from the heater; and by V_L and $S_L = \int V_L(t)\,dt$ when they are brought out along the length of the sample (Fig. 3). The instantaneous and integrated signals per turn across the corresponding pickup coil at the location of the voltage contacts are denoted by V_C and $S_C = \int V_C(t)\,dt$, respectively.

For brevity, we limit our discussion to measurements taken in zero applied magnetic field, unless stated otherwise. The two strip heaters were identical to each other, and, for the same initial conditions and heating rates, the above signals were independent of the strip heater used to destroy the magnetization of the sample. For all of the measurements, the amount of flux trapped in the sample before it was driven normal was the same unless indicated otherwise. This was ensured by initially cooling the sample through T_c to 4.2°K in the same applied field. Further, we verified that the amount of trapped flux was the same by simultaneously monitoring the integrated signal per turn S_C across the pickup coil when the sample was driven normal and the trapped flux expelled. We shall first discuss the results obtained when the sample was placed in a uniform applied magnetic field. From the measurements of signals across the different pickup coils on collapse of flux trapped in the sample, we found that the magnetic flux density was uniform over the length of the Nb cylinder between the pickup coils.

For a change of flux $\Delta\Phi$, the integrated signals across the voltage contact pairs are such that

$$S_N + S_S = S_C = \Delta\Phi/c. \tag{4.1}$$

The signals S_N, S_S, and S_L, however, differed dramatically. The following results were obtained for the two samples:

$$S_N = 0.927\Delta\Phi/c, \quad S_S = 0.073\Delta\Phi/c, \quad S_L = 0.423\Delta\Phi/c \tag{4.2}$$

for sample 1, thick wall;

$$S_N = 0.980\Delta\Phi/c, \quad S_S = 0.020\Delta\Phi/c, \quad S_L = 0.477\Delta\Phi/c \tag{4.3}$$

for sample 2, thin wall. The polarity of the integrated as well as the instantaneous signals is solely given by the direction of the trapped field. The results given by Eqs. (4.2) and (4.3) were also independent of the sign, viz., paramagnetic or diamagnetic, of the initial magnetic moment induced in the sample.[11,12] Thus the signals S_N, S_L, and S_S approach $\Delta\Phi/c$, $\Delta\Phi/2c$, and 0, respectively, with decrease in wall thickness of the cylinder.

We can identify two distinct contributions to the instantaneous signals V_N and V_S, one occurring during an initial short interval (t_0, t_1) and the other over a longer time interval (t_1, t_F), where the collapse of flux in the sample is assumed to start at $t = t_0$ and end at $t = t_F$. The top trace in Figs. 4 and 5 shows the signals V_N and V_S, respectively, for

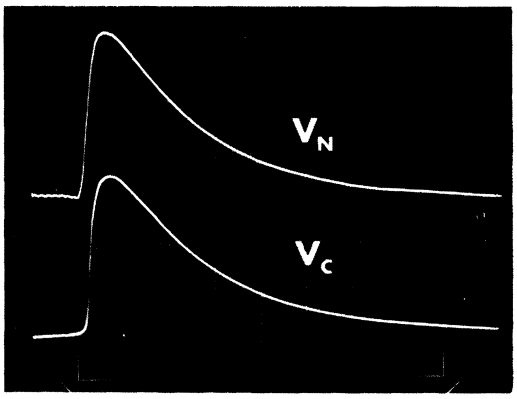

FIG. 4. V_N (upper trace) and V_C (lower trace) during initial stages of collapse of flux mainly from the hole of sample 1. Horizontal scale: 5 msec/division; vertical scale: 2 mV/division; $B_a = 1.594$ kG. See text for explanation of V_N and V_C.

sample 1 during the initial short interval (t_0, t_1) immediately after applying the voltage pulse to the heater. The bottom trace in these figures shows the signal V_C across the pickup coil at the location of the voltage contacts. We note the correspondence between V_N and V_C and also that $V_S \simeq 0$ during this interval. As we shall see shortly, the relatively large signals during this period indicate that a major fraction of the total flux in the sample existing mainly in the hole, collapses in this short initial interval.

Figures 6 and 7 show instantaneous signals over time interval (t_0, t_F) due to collapse of the entire flux initially trapped in sample 1. The bottom trace in Figs. 6 and 7 shows $-V_N$ and V_S, respectively, while the top trace shows the corresponding pickup-coil signal per turn V_C. The sweep rate is much slower and the voltage sensitivity much higher in the latter figures (cf. Figs. 4 and 5). The starting point of each trace is indicated by a white dot on the corresponding horizontal axis.

The occurrence of these signals, though much reduced, after the initial large signals V_N and V_C seen in Figs. 4 and 5 indicate a gradual decay of flux remaining in the sample wall. We note that the signal V_S continues to be negligibly small during and beyond the initial period (t_0, t_1) up to $t \simeq 200$ msec, when it increases and eventually attains a peak value at $t \simeq 640$ msec from the start.[13] A much reduced and decreasing signal V_N also attains a small peak value at the same instant $t \simeq 640$ msec. At this instant, a peak in the instantaneous signal V_C is also observed. We also note considerable structure in the signals V_C, V_N, and V_S during the entire period (t_1, t_F).

The gradual collapse of flux in the cylinder wall can be followed more closely in a quantitative analysis of the data shown in Figs. 6 and 7. Figure 8 shows the instantaneous signal $V_S(t)$ normalized to the corresponding signal $V_N(t)$. From Figs. 6–8, we see that V_S/V_N grows between the period from $t \simeq 200$ msec to $t \simeq 640$ msec such that

$$V_S/V_N \simeq 0 \quad \text{for} \quad t_0 < t \lesssim 200 \text{ msec} \tag{4.4}$$

and

$$(V_S/V_N)_{\max} \simeq 3.0 \quad \text{at} \quad t \simeq 640 \text{ msec}. \tag{4.5}$$

When the sample was placed in a nonuniform field, the flux it embraced at different points along its length varied strongly. From our measurements, however, we found that the observed signals still followed Eqs. (4.2) and (4.3). The sig-

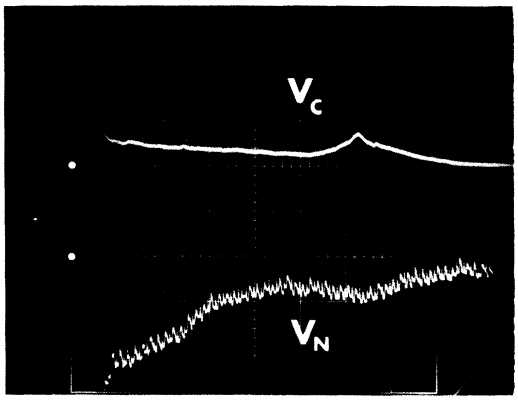

FIG. 6. V_C (upper trace) and $-V_N$ (lower trace) during complete collapse of flux in sample 1. Horizontal scale: 100 msec/division; upper trace: 0.08 mV/division; lower trace: 0.02 mV/division; $B_a = 1.594$ kG. V_C and $-V_N$ during initial stages of flux collapse, shown in Fig. 4, are here off scale.

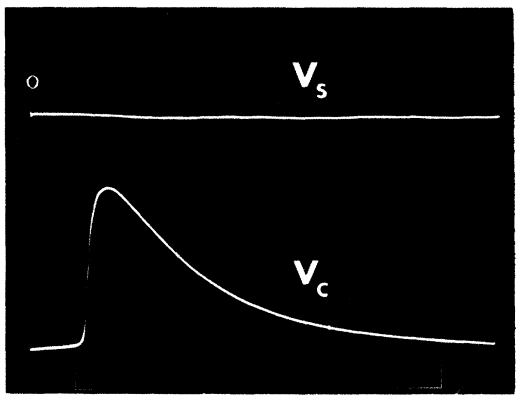

FIG. 5. V_S (upper trace) and V_C (lower trace) during initial stages of collapse of flux mainly from the hole of sample 1. B_a, time sweep and sensitivity as in Fig. 4.

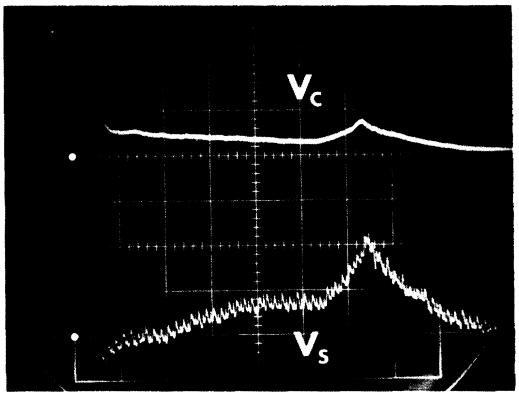

FIG. 7. V_C (upper trace) and V_S (lower trace) during complete collapse of flux in sample 1. B_a, time sweep, and sensitivity as in Fig. 6. V_C during initial stages of flux collapse, shown in Fig. 5, is here off scale.

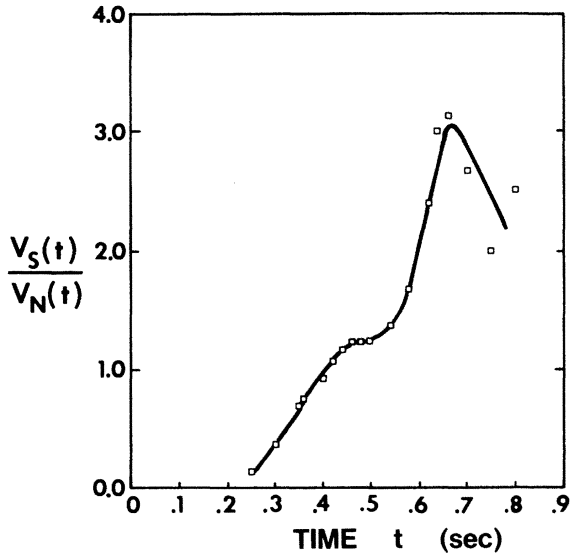

FIG. 8. Normalized instantaneous voltage $V_S(t)/V_N(t)$ versus time t during complete collapse of flux in sample 1.

nals across any pair of voltage contacts correspond to the flux trapped in the cylinder cross section at the location of those *contact* points.

Placing the sample in a nonuniform magnetic field permits a closer examination of the significance of both the location of the contact points and the configuration of the measuring leads. With this point of view, a special configuration of measuring leads was attempted for sample 2. In this arrangement, the voltage leads from the voltage contacts at location C [Fig. 3, inset (a)] were brought out a distance $L/4$ along the length and close to the outer surface up to location B. The voltage leads were then brought out close to and along the circumference toward one of the strip heaters. Let the flux trapped in the sample cross section at C and B be $\Delta\Phi_C$ and $\Delta\Phi_B$, respectively. The measured integrated signal S in this arrangement was found to be

$$S = S_L + \Delta\Phi_B/2c = (1/c)(0.477\Delta\Phi_C + 0.5\Delta\Phi_B), \qquad (4.6)$$

where the second equality follows from Eq. (4.3).

Flux collapse due to a localized perturbation. The dynamics of flux collapse due to a localized perturbation on the sample can be understood through the study of signals across the voltage contacts on our sample. These results are divided into two categories and are described here briefly.

(i) In one series of measurements of sample 2, we were interested in the direction of escape of flux, *mainly* from the cylinder hole, from the sample cross sections at a distance from the hairpin heater as the flux in the sample over the region of the hairpin heater collapsed. For this purpose, we studied the integrated signals across various pairs of contact points as described earlier, when the flux trapped in the cylinder over the part of its length in the vicinity of the hairpin heater was destroyed on application of a heat pulse to that heater [Fig. 3, inset (b)].

This also resulted in a total or partial collapse of flux to a varying extent over sample cross sections at a distance from the hairpin heater. The proportion of flux collapse in these regions was found to depend mainly on (i) the initial flux density over the sample cross section in the region of the hairpin heater, (ii) the power fed to the heater and the duration of the heat pulse, and (iii) the distance of the sample cross section under investigation from the heater. For a given sample cross section, the proportion of flux collapse appeared to depend upon the energy dissipated in the cylinder wall in the vicinity of the hairpin heater due to (i) collapse of flux in the region of the heater and (ii) heat transmitted from the heater.

Using the hairpin heater, we found that the integrated signal across a pair of voltage contacts *at a distance* from the heater, with measuring leads arranged around the circumference toward the side of the heater [contacts C, Fig. 3, inset (b)], corresponded to the total change of flux over that cross section, while the signal across the same contact points with leads taken out in the opposite direction was zero. These signals were essentially similar to the results discussed above for the initial period (t_0, t_1), although in the present case the heater was at a distance from the sample cross section at the location of the contacts. These results were independent of the initial flux density in the sample and were observed even when a comparatively low voltage pulse of a short duration, that was just sufficient to destroy flux in the hole of the sample near the heater region, was applied to the hairpin heater.

(ii) In a separate series of measurements on sample 1, the integrated signal across a pair of contact points at location B [Fig. 3, inset (a)], with measuring leads taken out around the circumference toward one side, and the integrated signal across the corresponding pickup coil at that location were measured simultaneously during spontaneous flux jumps as the applied magnetic field is swept over $0 \rightarrow H_{c2} \rightarrow 0$. It was noted that the integrated signal across the contact points corresponded to a fraction c of the total flux change over the sample cross section. Of course, the signal across these contact points with leads taken out in the opposite direction corresponded to a fraction $1 - c$ of the flux change. It is interesting to note that the fraction c varied randomly between zero

and unity (including the extreme values) for successive flux jumps. Similar measurements were also taken, simultaneously, at two locations, B and C, along the length of the sample. The integrated signal across contact points at location C, with measuring leads taken out in the same manner as at location B, corresponded to a fraction c' of flux change over the sample cross section at location C.

For a given flux jump, we found that $c \simeq c'$ generally. In particular, $c = c'$ during the first flux jump as the applied magnetic field along a virgin sample was increased (decreased) from $0 \rightarrow H_{c2}$ ($H_{c2} \rightarrow 0$). However, for subsequent flux jumps, $c \gtrless c'$ slightly for a small number of the flux jumps. In a few cases, c and c' differed dramatically from each other.

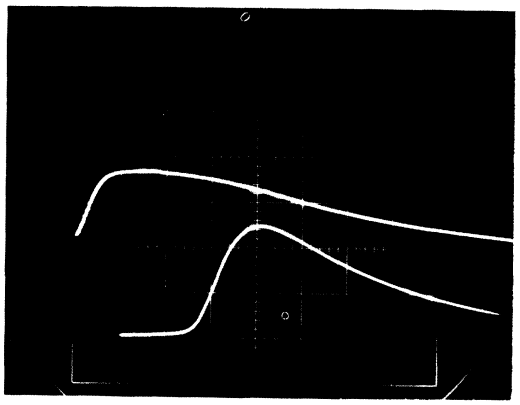

(a)

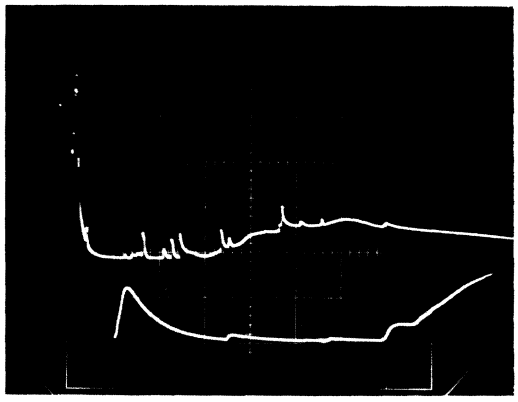

(b)

FIG. 9. Instantaneous voltage versus time across identical pick up coils wound around Nb sample 1 at two locations, C (upper trace) and B (lower trace) [see Fig. 3(a)], along its length during spontaneous flux jumps. (a) First flux jump suffered by the virgin sample as the applied magnetic field is increased from zero to 1.945 kG. Horizontal scale: 2msec/division; upper trace = 0, 1 V/division; lower trace = 0.1 V/division. (b) The next flux jump as the applied magnetic field is further increased to 3.112 kG. Horizontal scale: 1 msec/division; top trace: 0.2 V/division; lower trace: 0.1 V/division.

The upper and lower traces in Figs. 9(a) and 9(b) show the instantaneous signals induced across identical pickup coils wound around the waist of the Nb cylinder (sample 1) at two locations C and B, respectively [Fig. 3, inset (a)], along its length during two successive spontaneous flux jumps as the applied field was changed. The voltage traces in Fig. 9(a) correspond to the first flux jump suffered by the virgin sample as the external field was increased from zero. From these preliminary results, it appeared that, starting from a virgin sample, the first jump originated at the top or bottom end and propagated toward the midpoint of its length.[14] Thus, the flux jump at B lagged behind the flux jump at C. From Fig. 9(a), we estimate that the velocity of propagation of the flux jump along the length between B and C was $\sim 6 \times 10^2$ cm/sec (cf. corresponding results reported for 0.05-cm-diam Nb wire, $\sim 2 \times 10^4$ to 10^5 cm/sec).[15] Starting with a virgin sample, the first flux jump [Fig. 9(a)] appeared to consist of a single event while the successive jumps were always accompanied by a number of smaller flux jumps [Fig. 9(b)]. We also see from the lower trace of Fig. 9(b) that the sample cross section at B was more stable than that at position C.

V. CALCULATIONS OF FLUX-FLOW VOLTAGES IN A HOLLOW SUPERCONDUCTING CYLINDER

A. Problem definition

We follow the discussion of Sec. II for calculating the flux-flow voltages observed in the present experiment. Figure 10(a) shows schematically the cross section of a hollow cylinder with magnetic flux in the hole and the wall. The cross-shaded area on the right represents the region embraced by a strip heater. The voltage leads (which are shown at a distance from the cylinder for clarity) were actually held close to the outer surface of the cylinder such that the area enclosed between the leads and the cylinder was negligible.

Following Eqs. (2.1) and (2.2), if we choose $C_L = C_N$ for the signal V_N and $C_L = C_S$ for the signal V_S, then the second term in Eq. (2.1) is zero [see Fig. 10(a)] since

$$\Phi_{M_N N} = \int_{S_{M_N N}} \vec{B} \cdot \hat{n}\, dS = 0$$

and

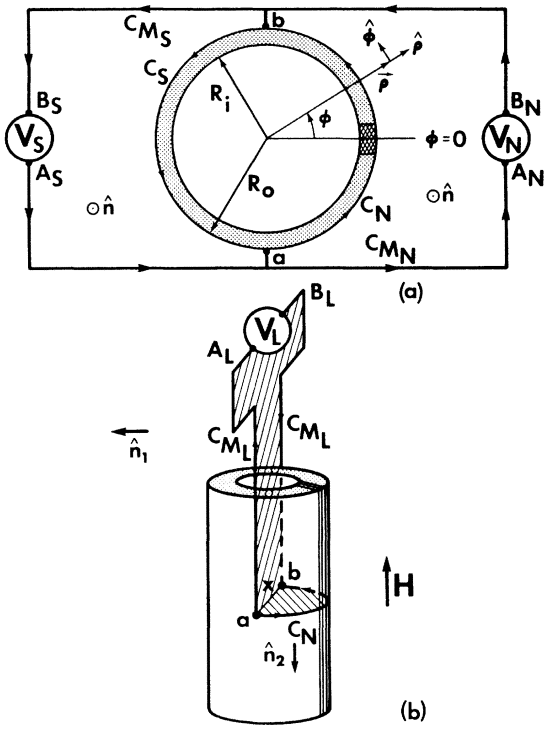

FIG. 10. (a) Schematic of sample cross section and lead arrangements for measurement of voltages V_S and V_N across two contact points a and b on the sample. (See Fig. 3.) The voltage leads are shown some distance from the cylinder only for visual clarity. (b) Configuration of voltage measuring leads when they are taken out along the length of the specimen from the two contact points for measurment of voltage V_L. The area bounded by the measuring leads and the chosen path C_N on the superconductor surface between the contact points is crosshatched. (See Fig. 3.)

$$\Phi_{M_S S} = \int_{S_{M_S S}} \vec{B}\cdot\hat{n}\, dS = 0,$$

and we have

$$V_N = V_{A_N} - V_{B_N} = \int_{a[C_N]}^{b} d\vec{l}\cdot\vec{E}' \tag{5.1}$$

and

$$V_S = V_{B_S} - V_{A_S} = \int_{b[C_S]}^{a} d\vec{l}\cdot\vec{E}'. \tag{5.2}$$

Using cylindrical coordinates (ρ, ϕ, z) and assuming that there is no z dependence, $d\vec{l} = R_0\, d\phi\, \hat{\phi}$, where R_0 is the outer radius of the cylinder and $\hat{\phi}$ is the unit vector in the ϕ direction, we have

$$V_N = R_0 \int_{-\pi/2}^{\pi/2} E'_\phi(R_0, \phi, t)\, d\phi \tag{5.3}$$

and

$$V_S = R_0 \int_{\pi/2}^{3\pi/2} E'_\phi(R_0, \phi, t)\, d\phi. \tag{5.4}$$

In the superconducting state

$$E'_\phi(R_0, \phi, t) = B_z(R_0, \phi, t) v_\rho(R_0, \phi, t)/c, \tag{5.5}$$

where $B_z(R_0, \phi, t)$ is the z component of the magnetic flux density (magnetic induction) and $v_\rho(R_0, \phi, t)$ is the ρ component of the velocity of vortices (each carrying flux $\phi_0 = hc/2e$) just inside the specimen's surface at the coordinates R_0, ϕ and time t. In the normal state, we may write, with the help of Ampere's law,

$$E'_{n\phi}(R_0, \phi, t) = \rho_n J_{n\phi}(R_0, \phi, t) = -\frac{D}{c}\left.\frac{\partial B_z(\rho, \phi, t)}{\partial \rho}\right|_{\rho=R_0}, \tag{5.6}$$

where $J_{n\phi}$ is the current density, $D = \rho_n c^2/4\pi$ is the magnetic diffusivity, and the subscript n denotes the normal state.

Examining Eqs. (5.1)–(5.4), we see that the central problem in obtaining V_N and V_S is the determination of E'_ϕ for different conditions using Eqs. (5.5) and (5.6).

B. Systematics of flux change in a hollow superconducting cylinder

To simplify this discussion, we first consider the case where magnetic flux is trapped in the hole and wall of the cylinder by cooling it in a uniform static initial magnetic field $H_a = H_a \hat{z}$ along the axis of the cylinder which is subsequently reduced directly to zero. Magnetization measurements on these samples indicate that the flux-retaining persistent current flows in a small layer of depth X_p at the outer surface of the cylinder. For simplicity, we use Bean's critical-state model, where the critical current density in this layer and hence the gradient of flux density is assumed to be independent of local magnetic induction. With the applied field H_a reduced to zero, $B_z(R_0, \phi) = 0$. Experimentally, we have also checked that $B_z(\rho, \phi) = B_a = H_a$ for $\rho \le R_i$, where R_i is the inner radius of the cylinder. Figure 11(a) shows the profile of magnetic induction $B = B_z$ initially present across the sample cross section. It can easily be seen that B_z is spatially uniform in the hole and over most of the wall thickness of the cylinder. Separate measurements of the flux trapped at different points along the length indicate that B_z has no z dependence. Since $X_p \ll R_0$, the magnetic flux $\phi(t)$ initially trapped in the sample at time $t = t_0$ is given by

$$\Phi(t_0) \simeq (\pi R_0^2 - \pi R_0 X_p) B_a. \tag{5.7}$$

Our results indicate that the collapse of flux in

a thin-wall hard superconducting cylinder takes place over three overlapping time intervals, which we refer to as time intervals I, II, and III. On application of a voltage pulse to the strip heater at time $t=t_0$, the region of the cylinder wall near $\phi=0$ in the immediate vicinity of the heater is heated through supercritical mixed states to the normal state. During time interval I, with $t_0<t<t_I$, the azimuthal persistent currents supporting the flux in the hole collapse rapidly and magnetic flux flows out of the sample through the heated region. The flux density B_{iz} in the hole of the specimen ($\rho<R_i$) decreases quickly to a value close to zero. We can easily show that $B_{iz}(\rho,\phi,t)$ is also spatially uniform.

Figure 11(b) shows the profile of magnetic flux density across a cross section of the cylinder wall at some distance from the strip heater at the end of interval I. As can be verified easily, $B_{iz}\ll B_a$ and is shown to be zero in this diagram. Our magnetization measurements also indicate that the magnitudes of the slopes of flux profiles at the inner and outer surfaces are the same.

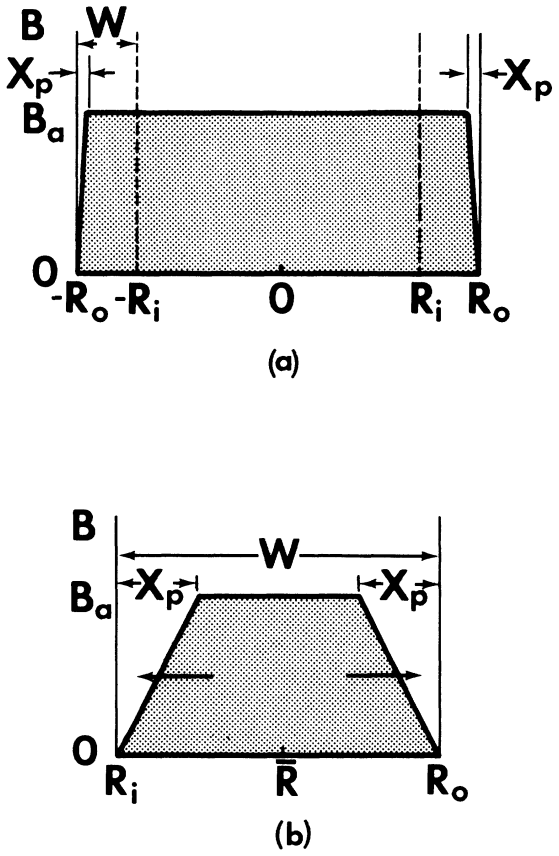

FIG. 11. Sketches of profile of magnetic induction (a) across the cross section of the hollow Nb cylinder trapped initially at $t=t_0$; (b) across the wall of the Nb cylinder after flux from the hole has escaped.

There are two other regions besides the hole of the cylinder from which magnetic flux is expelled during interval I: a small layer of depth X_p near the inner surface of the cylinder wall and the wall region embraced by and in the immediate vicinity of the strip heater. Both of these contributions are small by comparison with the decay of flux from the hole and will be ignored for the calculation of induced voltages in interval I alone (see Sec. V.C).

In order to calculate the decay rate of flux in the hole, we assume that the time interval is sufficiently short such that the arc length l_n of the heated normal region of the wall does not grow much beyond the immediate vicinity of the strip heater. That is, we assume that $l_n\approx l_{nI}$, a constant over time interval I or that $\dot{l}_n\tau/l_n\ll 1$, where $\dot{l}_n$ gives the time rate of change of l_n and τ is a time constant for the decay of flux in the hole. This assumption is well supported by our results.

The current I'_ϕ circulating in the ϕ direction per unit length of the cylinder of wall thickness W is given by Ampere's law,

$$B_{iz}=(4\pi/c)I'_\phi=(4\pi/c)J_{n\phi}W, \tag{5.8}$$

where the current density $J_{n\phi}$ in the normal heated region is assumed to be uniform over the wall thickness. We assume that the current I'_ϕ flows without dissipation in the critical-state region of the superconductor. Thus, $E'_\phi=0$ over most of the perimeter of the cylinder which is in the superconducting state, but

$$E'_\phi=E'_{n\phi}=\rho_n J_{n\phi}=DB_{iz}/cW \tag{5.9}$$

in the normal region.

The line integral around the contour C_i of inner radius R_i in the counterclockwise direction can be evaluated from Faraday's law and Eq. (5.9), which yields

$$\frac{dB_{iz}}{dt}=\frac{-Dl_n}{\pi R_i^2 W}B_{iz}. \tag{5.10}$$

Taking $l_n=l_{nI}$ to be a constant over interval I, we get

$$B_{iz}=B_a e^{-t/\tau}, \tag{5.11}$$

where

$$\tau=\pi R_i^2 W/Dl_{nI}. \tag{5.12}$$

Thus, the flux density B_{iz} in the hole should decay exponentially with a time constant τ which depends on the sample properties and dimensions.

Next, we focus our attention on time intervals II and III, during which flux in the wall collapses. After the initial time interval I, we assume that the interfaces between the superconducting state

and normal state at $\phi = +\phi_n(t)$ and $\phi = -\phi_n(t)$ move rigidly with angular velocities $\dot{\phi}_n(t)$ and $-\dot{\phi}_n(t)$. Ahead of each advancing superconducting-normal interface is an arc length of wall Δl that is heated sufficiently far above its original temperature that initially pinned vortices are depinned and driven towards the inner and outer wall surfaces. We refer to such supercritical regions as thermal fronts. The angular coordinates of the leading edges of the thermal fronts are $\pm(\phi_n + \Delta\phi)$. We define the time interval II ($t_I < t < t_{II}$) as that required for the normal region, of arc length $l_n = \bar{R}(2\phi_n)$, where $\bar{R} = (R_i + R_0)/2$ is the average wall radius, to grow from l_{nI} to $l_n = \pi\bar{R}$. Thus, at the end of this interval, the cylinder wall over the range $\phi = (-\pi/2, \pi/2)$ is in the normal state. Finally, during the time interval III ($t_{II} < t < t_{III}$), the normal region grows from $l_n = \pi\bar{R}$ to $l_n = 2\pi\bar{R}$. At time $t = t_{III}$ the entire flux originally trapped in the sample is collapsed.

As the thermal front advances, the unpinned vortices from the heated region migrate to and collapse at nearby inner and outer surfaces of the cylinder. Khanna and LeBlanc[6] have extensively studied the dependence of flux migration upon flux profiles and temperature gradients in type-II superconductors. In the present experiment, since the sample is essentially being heated equally and simultaneously, and hence symmetrically, at its inner and outer surfaces, equal numbers of vortices will migrate toward and collapse at the two surfaces. Thus the unpinned fluxoids with $\rho < \bar{R}$ migrate to the inner surface and annihilate at $\rho = R_i$, thus dumping their flux in the hole, while the unpinned vortices with $\rho > \bar{R}$ migrate to the outer surface and collapse at $\rho = R_0$ [see Fig. 11(b)].

In each advancing thermal front, the amount of flux collapsing from the wall at $\rho = R_i$ in time dt is $\frac{1}{2}(W - X_p)B_a v_n dt$ where, assuming $\Delta\phi$ to be constant, $v_n = \bar{R}\dot{\phi}_n$ is the speed of the thermal front. The net rate of change of flux in the hole at $\rho < R_i$ is equal to the rate at which liberated trapped flux at *both* thermal fronts collapses at the inner surface minus the rate at which flux leaks out across the normal region. From the resulting rate equation and Eq. (5.9) we obtain

$$\frac{dB_{iz}}{dt} + \frac{l_n D B_{iz}}{\pi R_i^2 W} = \frac{B_a}{2\pi R_i^2}(W - X_p)\dot{l}_n, \tag{5.13}$$

where $l_n = 2\bar{R}\phi_n$.

Equation (5.13) holds approximately for time interval I, when $B_{iz} \approx B_a$ and the term on its right-hand side is negligible in comparison with the other terms, such that Eq. (5.10) holds. In time interval II, however, B_{iz} drops to a small value by comparison with B_a. Furthermore, dB_{iz}/dt is then governed by the rate of change of l_n rather than by τ and can be shown to be negligible. This indicates that a steady state is quickly attained after the flux initially trapped in the hole has escaped. Thus, when $t \gg \tau$, the rate of addition of flux to the hole due to flux collapsing at $\rho = R_i$ is balanced by escape of flux through the heated normal region l_n. Equation (5.13) then yields

$$B_{iz} \simeq \frac{W(W - X_p)}{2D}\frac{\dot{l}_n}{l_n}B_a. \tag{5.14}$$

We have assumed that the angular width $\Delta\phi$ of each thermal front (the region of the cylinder wall under transition from the pinned superconducting to the normal state) is small compared with that of the normal region; i.e., $\Delta\phi \ll \phi_n$. In practice, the thermal front may be rather diffuse. However, Eq. (5.13) is still valid, provided the thermal fronts move rigidly with velocities $+\dot{\phi}_n$ and $-\dot{\phi}_n$.

Figure 12 shows schematically the current-density pattern in the vicinity of the thermal front at $\phi \approx \phi_n(t)$. The arrows on the contours of constant B show the direction of the local current density. The current density is essentially uniform in the normal region, but flows in the directions shown in the superconducting region, which is mostly in the critical state. The vortices that are unpinned because of the local increase in temperature experience a local Lorentz force in the direction of the small arrows in the diagram. The local electric field $\vec{E}' = \vec{B} \times \vec{v}/c$ has a large value only over the range Δl in the directions shown. From Fig. 12, we note that Δl is at least of order W but may be considerably larger if the thermal front is diffuse.

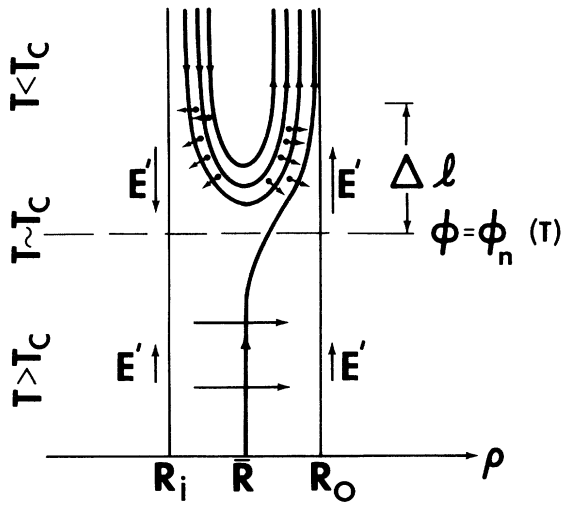

FIG. 12. Sketch of the current-density pattern and induced electric fields in and near the thermal-front regions of the cylinder wall.

C. Instantaneous and integrated voltages

1. Signals V_N, V_S, V_C, S_N, S_S, and S_C

From Faraday's law, we have [see Fig. 10(a) and Eqs. (5.1) and (5.2)]

$$V_C = -\frac{1}{c}\frac{d\phi(t)}{dt} = V_N + V_S, \tag{5.15}$$

where $d\phi(t)/dt$ is the rate of change of flux in the region $\rho < R_0$; V_C can be expressed as a line integral of $\vec{E}'$ in a counterclockwise direction around a contour C_0 of radius R_0 and is measured by the signal per turn across a pickup coil of radius $\simeq R_0$ wound around the sample. The voltages V_N and V_S during the various intervals can be calculated using the instantaneous value of E' over the appropriate arc length of the cylinder. The superscript on a time-integrated signal S will indicate the time interval over which the corresponding voltage is integrated.

(i) *Interval I*: Since $E'_\phi(R_0, \phi, t) = 0$ over the path C_S, we obtain from Eq. (5.2)

$$V_S = 0. \tag{5.16}$$

From Eqs. (5.9), (5.10), and (5.15) we obtain

$$V_N = V_C = (l_n D/cW) B_{iz}, \tag{5.17}$$

where we have ignored the loss of flux from the wall.

The initial rise in V_N or V_C corresponds to the rapid rise of l_n from 0 to l_{nI} while $B_{iz} \approx B_a$. Thus, the peak value of these signals is

$$(V_N)_{peak} = (V_C)_{peak} \simeq (D/cW) l_{nI} B_a. \tag{5.18}$$

As discussed earlier, the flux in the hole then decays exponentially with a time constant τ, provided $l_n = l_{nI}$, a constant. Thus

$$V_N = V_C \simeq (D/cW) l_{nI} B_a e^{-t/\tau}. \tag{5.19}$$

The time-integrated signals are

$$S_N^I = S_C^I \simeq (\pi R_i^2 + \pi R_i X_p) B_a / c \tag{5.20}$$

and

$$S_S^I = 0. \tag{5.21}$$

(ii) *Interval II*: Since, if $\Delta\phi \ll \phi_n$, the thermal fronts are confined to $|\phi| < \pi/2$, $E'_\phi(R_0, \phi, t) = 0$ over the path C_S and

$$V_S = 0. \tag{5.22}$$

The average electric field E'_ϕ at $\rho = R_0$ due to collapse of liberated flux at each of the thermal-front regions of arc length $\Delta l = \bar{R}\Delta\phi$ at $\phi = \pm\phi_n$ is

$$E'_\phi(R_0, \phi, t) = (W - X_p) B_a \dot{l}_n / 4c(\Delta l). \tag{5.23}$$

From Eqs. (5.9) and (5.14) we see that $E'_{n\phi}$ in the normal region l_n is

$$E'_{n\phi}(R_0, \phi, t) = (W - X_p) B_a \dot{l}_n / 2c l_n. \tag{5.24}$$

Using Eqs. (5.1), (5.23), and (5.24) we thus obtain

$$V_N = V_C = (W - X_p) B_a \dot{l}_n / c. \tag{5.25}$$

We note that the total contribution to V_N from the two thermal-front regions at $\phi = \pm\phi_n$ equals that from the normal region l_n. This occurs because equal amounts of liberated trapped flux in the thermal-front regions collapse at $\rho = R_0$ and $\rho = R_i$. The flux collapsing at $\rho = R_0$ produces an electrical field of large magnitude only near the thermal fronts. The flux collapsing at $\rho = R_i$, however, pumps flux into the hole which leaks out again at essentially the same rate through the entire length of the normal region l_n, such that $dB_{iz}/dt \simeq 0$. The resulting electric field $E'_\phi(R_0, \phi, t)$ around the outer surface of the cylinder is schematically shown in Fig. 13(a).

Recalling that $l_n \simeq l_{nI}$ at $t = t_I$ and $l_n = \pi\bar{R}$ at $t = t_{II}$ and assuming that $\Delta l \ll \pi\bar{R}$ and $l_{nI} \ll \pi\bar{R}$, we obtain for the time-integrated signals in interval II

$$S_N^{II} = S_C^{II} \simeq \pi\bar{R}(W - X_p) B_a / c, \tag{5.26}$$

$$S_S^{II} = 0. \tag{5.27}$$

(iii) *Interval III*: Figure 13(b) shows schematically the electric field $E'_\phi(R_0, \phi, t)$ in the time interval III, when the thermal fronts are confined to $|\phi| > \pi/2$ and $\phi_n > \pi/2$. As in interval II [see Eq. (5.25)]

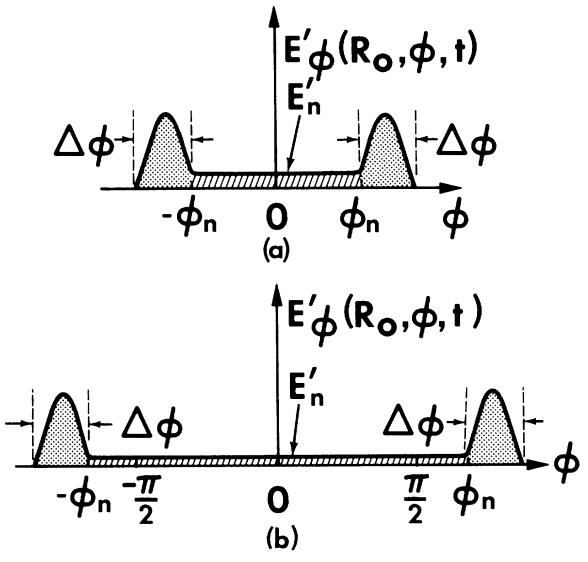

FIG. 13. Sketch of the induced electric field in the normal (crosshatched) and thermal-front (shaded) regions of the cylinder wall (a) during interval II and (b) during interval III. In each case, the total area under the curve in the two humps, corresponding to the thermal fronts, equals the area under the flat portion, corresponding to the heated normal region.

$$V_C = (W - X_p) B_a \dot{l}_n / c. \tag{5.28}$$

Further, using Eqs. (5.23) and (5.24), we obtain

$$V_N \simeq \frac{\pi \bar{R}(W - X_p) B_a}{2c} \frac{\dot{l}_n}{l_n}, \tag{5.29}$$

$$V_S \simeq \frac{(W - X_p) B_a \dot{l}_n}{c} \left(1 - \frac{\pi \bar{R}}{2 l_n}\right). \tag{5.30}$$

At the beginning of interval III, $\phi_n = \pi/2$ and $l_n = \pi \bar{R}$, such that

$$V_S = V_N = \tfrac{1}{2} V_C. \tag{5.31}$$

At the end of the interval III, when $l_n = 2\pi \bar{R}$, we obtain, provided $\Delta\phi \ll \phi_n$ and $\Delta l \ll l_n$,

$$V_S = 3 V_N = \tfrac{3}{4} V_C. \tag{5.32}$$

The time integrals of the induced signals over interval III are

$$S_N^{\mathrm{III}} \simeq \pi \bar{R}(W - X_p) B_a (\ln \sqrt{2})/c, \tag{5.33}$$

$$S_S^{\mathrm{III}} \simeq (1 - \ln \sqrt{2})[\pi \bar{R}(W - X_p) B_a / c], \tag{5.34}$$

and

$$S_C^{\mathrm{III}} \simeq \pi \bar{R}(W - X_p) B_a / c. \tag{5.35}$$

Thus,

$$\frac{S_N^{\mathrm{II}} + S_N^{\mathrm{III}}}{S_S^{\mathrm{II}} + S_S^{\mathrm{III}}} = \frac{1 + \ln \sqrt{2}}{1 - \ln \sqrt{2}} = 2.06 \tag{5.36}$$

and

$$\frac{S_S^{\mathrm{III}}}{S_N^{\mathrm{III}}} = \frac{1 - \ln \sqrt{2}}{\ln \sqrt{2}} = 1.885. \tag{5.37}$$

The total integrated signal due to the collapse of the entire flux in the sample is

$$S_C = \frac{\Phi(t_0)}{c} \simeq \frac{(\pi R_0^2 - \pi R_0 X_p) B_a}{c} \tag{5.38}$$

and the ratios of the signals S_S and S_N, integrated over all three time intervals, to S_C are

$$\frac{S_S}{S_C} = \frac{S_S^{\mathrm{III}}}{S_C} \simeq \frac{(1 - \ln \sqrt{2}) \bar{R}(W - X_p)}{R_0 (R_0 - X_p)} \tag{5.39}$$

and

$$S_N / S_C = 1 - S_S / S_C. \tag{5.40}$$

2. *Signals V_L and S_L*

The time-integrated signal S_L, where the measuring leads from the voltage contacts on the cylinder surface are taken out along the length of the cylinder, provides an interesting example of the roles of contributions due to different terms in Eq. (2.1). Since the leads are along the direction of flux density in the sample, one might incorrectly expect S_L to be zero. However, following our earlier discussion, we can calculate it easily and find it not to be zero.

In Eq. (2.1), if we choose $C_L = C_N$ and $C_M = C_{M_L}$ [see Fig. 10(b)],

$$V_L = V_{A_L} - V_{B_L} = \int_{a[C_N]}^{b} d\vec{l} \cdot \vec{E}' - \frac{1}{c} \frac{d\Phi_{M_L N}}{dt}. \tag{5.41}$$

There are two contributions to the magnetic flux $\Phi_{M_L N}$ through the surface bounded by the paths C_{M_L} and C_N: (i) the flux through the surface bounded by the paths C_{M_L} and bxa in the direction of unit normal $\hat{n}_1$ to this surface, which is very nearly zero by symmetry, and (ii) the flux through the surface bounded by the paths axb and C_N in the direction of unit normal $\hat{n}_2$ as shown in Fig. 10(b). Thus,

$$\Phi_{M_L N}(t_0) = -\tfrac{1}{2} \Phi(t_0). \tag{5.42}$$

Using Eq. (5.41), we find the time-integrated signal S_L to be

$$S_L = S_N - \Phi(t_0)/2c \tag{5.43}$$

or, from Eq. (5.38),

$$S_L / S_C = S_N / S_C - \tfrac{1}{2}. \tag{5.44}$$

From Eq. (5.44), we see that, with the above arrangement of the measuring leads, both terms on the right-hand-side of Eq. (2.1) produce important contributions to the induced voltage.

VI. COMPARISON WITH EXPERIMENTAL RESULTS AND DISCUSSIONS

A. Instantaneous and integrated signals

Salient features of our model can be tested experimentally and are in excellent agreement with our experimental results. As noted earlier, the different time intervals overlap to some extent, and it is difficult to exactly identify each interval with the corresponding signal. Both the instantaneous and integrated signals provide important results regarding the origin of induced voltages due to vortex motion in superconductors. A study of signals S_N and S_S integrated from the start to finish of flux collapse provides a good overall test of our model, and the instantaneous and integrated signals over a given time interval provide added insight into the mechanism of flux decay in our sample.

Interval I: For a given change of flux, the dramatic results for the signals V_N and V_S given by Eqs. (5.16) and (5.17) are in good agreement with the experimental results shown in Figs. 4 and 5, respectively. In particular, we note the important experimental result that $V_S = 0$ and $V_N = V_C$ during decay of flux mainly from the hole of the cylinder. The time constant τ for exponential

decay of signals V_N and V_C and hence the arc length l_{nI} of heated normal region are nearly constant. From Fig. 4, we find that $\tau = 12$ msec at $(V_N)_{peak}$ and soon settles to a constant value of $\tau = 10$ msec.

Using Eq. (5.12), $\tau = 12$ msec, and near the transition temperature for Nb $\rho_n = 0.8\ \mu\Omega - \text{cm}$, we find $l_{nI} = 1.56$ cm, which is about three times the width of the strip heater. Using this value of l_{nI} and the experimental value $B_a = 1.594$ kG, we determine from Eq. (5.18) $(V_N)_{peak} = 8.0$ mV, which compares well with the experimental value of 7.4 mV. The difference in the experimental and calculated values of $(V_N)_{peak}$ may be due to our assumption that l_n changes from zero to l_{nI} while B_{tz} remains constant. We would expect a small leakage of flux, thus making $B_{tz} < B_a$ as l_n grows quickly but continuously from zero to l_{nI}.

Intervals II and III: We now discuss the signals induced due to escape of flux from the wall. From magnetization measurements, we calculate that (Fig. 11)

$$X_p = 0.0135 \text{ cm} \quad \text{for sample 1}$$

and

$$X_p = 0.0088 \text{ cm} \quad \text{for sample 2.}$$

Correcting for escape of flux from region l_{nI} of the wall during interval I, the modified Eqs. (5.26) and (5.36) are

$$S_N^{II} = (1/c)(\pi\bar{R} - l_{nI})(W - X_p)B_a$$

and

$$\frac{S_N^{II} + S_N^{III}}{S_S^{II} + S_S^{III}} = \frac{1 - l_{nI}/\pi\bar{R} + \ln\sqrt{2}}{1 - \ln\sqrt{2}}. \tag{6.1}$$

Experimentally, we find for sample 1

$$(S_N^{II} + S_N^{III})/(S_S^{II} + S_S^{III}) = 1.60 \tag{6.2}$$

by integrating the area under the voltage traces in Figs. 6 and 7 from time $t = 60$ msec to $t = t_F = 1000$ msec. Combining Eqs. (6.1) and (6.2) and solving for l_{nI}, we obtain $l_{nI} = 1.41$ cm, which is to be compared with the value $l_{nI} = 1.56$ cm obtained above by a different method. Owing to overlap of intervals I and II, it is difficult to completely separate the contributions to the observed signal due to collapse of flux from the hole and wall of the cylinder.

From Fig. 8, the time t corresponding to the start of interval III at $V_S/V_N = 1$ [see Eq. (5.31)] is estimated to be 400 msec. By integrating the area under the voltage traces in Figs. 6 and 7 from time $t = 400$ msec to $t = t_F = 1000$ msec to obtain S_S^{III} and S_N^{III}, we obtain

$$S_S^{III}/S_N^{III} = 1.89, \tag{6.3}$$

which compares very well with the calculated value 1.89 given by Eq. (5.37).

Further, from Fig. 8, we note that at $t \approx 640$ msec

$$V_S(t)/V_N(t) \simeq 3.0, \tag{6.4}$$

as expected from our model at the end of time interval III [Eq. (5.32)]. It indicates that the leading edges of two thermal fronts traveling with velocity $\dot{\phi}_n$ and $-\dot{\phi}_n$ meet at $\phi = \pi$ at $t \simeq 640$ msec.

Integrated Signals S_N, S_S, and S_L: A comprehensive test of our model is provided by the study of signals S_N, S_S, and S_L integrated over all three time intervals as all trapped flux in the sample is expelled. Using Eqs. (5.39), (5.40), and (5.44), we find that on the basis of the present model:

$$\frac{S_N}{S_C} = 0.927, \quad \frac{S_S}{S_C} = 0.073, \quad \frac{S_L}{S_C} = 0.427 \tag{6.5}$$

for sample 1, thick wall;

$$\frac{S_N}{S_C} = 0.976, \quad \frac{S_S}{S_C} = 0.024, \quad \frac{S_L}{S_C} = 0.476 \tag{6.6}$$

for sample 2, thin wall. Recalling that $S_C = \Delta\phi/c$, these results compare very well with our experimental results given in Eqs. (4.2) and (4.3).

From Fig. 7, we note that V_S and S_S have a small nonzero value over the period from $t \simeq 200$ msec to $t \simeq 400$ msec contrary to our model, where $V_S^I = V_S^{II} = 0$ and $S_S^I = S_S^{II} = 0$. This indicates a diffuse thermal front during intervals I and II which has coordinate $|\phi| > \pi/2$ while $\phi_n < \frac{1}{2}\pi$ and $l_n < \pi\bar{R}$ during this period.

The measured signals with the special configuration of measuring leads [Eq. (4.6)] can easily be explained from our discussion in Sec. V C2. The surface bounded by the measuring leads now encloses half the flux trapped in the sample cross section at position B [Fig. 3, inset (a)] in addition to the case discussed in Sec. V C2. Further, the collapse of this flux aids the signal S_L across the contact points at position C, thus leading to results given by Eq. (4.6). This measurement clarifies the importance of location of the contact points and configuration of the voltage measuring leads in the study of flux-flow voltages in superconductors and thus stresses the contributions to flux-flow voltages from each of the two terms in Eq. (2.1).

We note the small structure present in all signals, V_C, V_N, and V_S, over the period (t_1, t_F). Preliminary studies indicate that these structures may be due to the occurrence of macrovortices[17,18] in the wall of the sample as flux in the wall is destroyed by heating through the strip heater.

The sharp peak in signals V_C, V_N, and V_S at $t \simeq 640$ msec (Figs. 6 and 7) indicates an increase in rate of collapse of flux from the wall when the

two thermal fronts traveling with angular velocities $\dot{\phi}_n$ and $-\dot{\phi}_n$ meet at $\phi = \pi$. For times t from the start until about 640 msec, the wall region ahead of the thermal front is essentially at 4.2 °K and serves as a cold sink to conduct away the heat from the thermal front. At $t \approx 640$ msec, the leading edges of the two thermal fronts reach $\phi = \pi$ from opposite directions, giving rise to a more rapid rate of temperature increase at $\phi = \pi$ and a greater rate of depinning of the trapped vortices. For times $t \gtrsim 640$ msec, the last remaining vortices become depinned and collapse at the surfaces. Finally, at $t = t_F$, all flux in the wall has been expelled and the wall is entirely normal. We do not fully understand, however, the decrease of the ratio V_S/V_N to values less than 3 for $t > 640$ msec. The experimental results that $V_S/V_N \approx 2$ at $t = 800$ msec indicates an approximately 30% increase in the amount of flux collapsing at the inner surface over that expected for symmetric flux flow. Why flux flow out of the advancing thermal fronts becomes asymmetric near $\phi = \pi$ at $t \simeq t_F$, although it is apparently symmetric at earlier times, remains an unanswered question.

B. Flux collapse due to a localized perturbation

(i) It is clear from earlier discussion that the integrated signal across a pair of contact points combined with a measurement of the change of flux indicates the direction of escape of flux from the hole. The "weak spots" on the cylinder wall can thus be identified.

From results obtained using the hairpin heater, we find that flux from those regions which are *at a distance* from the site of thermal perturbation also escapes through the same half of the cylinder wall in which the hairpin heater is located, even when the perturbation is very weak.

(ii) The results of induced signals across a pair of contact points at a given cross section of the sample during flux jumps indicate that flux leaks with equal probability from each half of the circumference at that location. This suggests that the weak spots are randomly distributed around the circumference.

Similar observations taken simultaneously at two positions along the length indicate that usually equal amounts of flux escape through the same half circumference along the entire length of the cylinder during a flux jump. This is always the case for the first flux jump.

From above results (i) and (ii), it would appear that collapse of flux in different parts of length of the cylinder are "coupled" together. The collapse of persistent currents at one site on the cylinder wall "induces" their collapse in its proximity through thermal and electromagnetic coupling mechanisms. This appears to be particularly valid when the trapped flux in the sample is uniform.

With nonuniform flux density in the sample, as would be expected after redistribution of trapped flux following a flux jump, various regions of the cylinder wall over a given cross section are in different subcritical states. The location and nature of the subsequent flux jump may then also depend on these subcritical states along with the proximity-induced effects. This is supported by our observations that in any subsequent jump after the first flux jump, the proportion of flux escaping from the sample in any direction *may not* be the same over its entire length, and indeed may be quite different in some cases (also see Ref. 12). Further, we note that such flux jumps are invariably followed by a succession of small flux jumps over a given cross section, as would be expected from the above discussion [see Fig. 9(b)]. Further investigations are needed to fully understand flux-jump phenomena in hollow Nb cylinders.

VII. CONCLUSIONS

The instantaneous and integrated signals across a fixed pair of contacts attached to the surface of a hollow superconducting Nb cylinder, when a fixed amount of magnetic flux $\Delta\phi$ threading the hole and wall of the cylinder was changed, were found to depend dramatically on the configuration of the voltage measuring leads relative to direction of flux motion. When the flux in the hole was collapsed by heating the cylinder wall over a narrow strip along its entire length, the observed signals with measuring leads brought out *toward* the heated strip corresponded to the total change of flux in the hole. During the exit of flux from the hole, the signals with measuring leads brought out away from the heated strip were negligibly small. Subsequent collapse of flux in the wall of the cylinder led to signals across the contact points with measuring leads brought out toward *either* side of the heated region of the cylinder wall. These signals were related to the flux change in the wall in a complicated manner. The integrated signal across the contact pair with measuring leads brought out along the length of the cylinder corresponded to approximately half of the flux initially trapped in the sample.

In explaining these results, we pursued the viewpoint that the motion of vortex segments within the interior of the superconducting body does not contribute to our measured signals and we considered two contributions to the measured voltages: (i) the signal due to the generation of a flux-motion-induced electric field along an arbitrary path through

the superconductor between the contact points, and (ii) the signal due to the change of flux through the surface bounded by the chosen path and the measuring leads. Taking both of these contributions into account, we discussed the contribution to the flux-flow voltage from a moving vortex. We concluded that the measured flux-flow voltages in general depend upon the position of the contact points on the surface of the superconductor and the configuration of the measuring leads relative to the direction of magnetic induction and flux motion in the superconductor.

In the present experiment, both of the above contributions to the measured signals depended upon the direction of flux motion in the superconductor. We exploited the concept of critical flux gradients to visualize the collapse of flux from the hole and wall of the cylinder and developed a formalism from which the expected signals could be calculated. Good agreement between the calculated and measured values was found.

Finally, we showed how measurements of signals across pairs of contact points with measuring leads arranged on one side along its circumference could be used to study flux jump in a hollow superconducting cylinder.

ACKNOWLEDGMENTS

One of the authors (S.M.K.) would like to thank Dr. Eugene W. Urban of Space Sciences Laboratory, Marshall Space Flight Center, for constant encouragement and valuable discussions. He is also indebted to the National Academy of Sciences/National Research Council and to NASA, George C. Marshall Space Flight Center, for their support. Another author (J.R.C.) thanks Professor G. Eilenberger for his hospitality at the Institut für Festkörperforschung of the Kernforschungsanlage Jülich, where some of this work was carried out.

---

*Prepared in part for the U.S. Energy Research and Development Administration under Contract No. W-7405-eng-82.

†NRC/NASA Postdoctoral Resident Research Associate. Present address: Physics Department, University of Ottawa, Ottawa, Canada.

‡Senior Fulbright-Hays Research Scholar.

[1]For an excellent review of this subject, see Y. B. Kim and M. J. Stephen, in *Superconductivity* edited by R. D. Parks (Dekker, New York, 1969), Vol. 2, p. 1107.

[2]B. D. Josephson, Phys. Lett. 16, 242 (1965).

[3]J. G. Park, J. Phys. F 2, 957 (1972).

[4]J. G. Park, J. Phys. C 2, 742 (1969).

[5]J. R. Clem, Phys. Rev. B 1, 2140 (1970).

[6]S. M. Khanna and M. A. R. LeBlanc, J. Appl. Phys. 43, 5165 (1972); J. Phys. F. 4, 550 (1974).

[7]J. Lowell, J. S. Munoz, and J. B. Sousa, Phys. Rev. 183, 497 (1969); Phys. Lett. 24A, 376 (1967); A. T. Fiory and B. Serin, Phys. Rev. Lett. 16, 308 (1966); 19, 227 (1967); P. R. Solomon and F. A. Otter, Jr., Phys. Rev. 164, 608 (1967); R. P. Huebener and A. Seher, *ibid.* 181, 701 (1969).

[8]P. Jarvis and J. G. Park, J. Phys. F 4, 1238 (1974).

[9]J. Lowell S. Parkinson, and A. C. Rose-Innes, J. Low Temp. Phys. 8, 277 (1972).

[10]S. M. Khanna and M. A. R. LeBlanc, IEEE Trans. Magn. MAG-11, 354 (1975).

[11]We always check that for a change of flux $\Delta\Phi$ caused by a change in the applied magnetic field along the Nb tube in the normal state, the integrated signal $S_L = 0$ and each of the integrated signals with measuring leads taken out towards opposite sides of the circumference equals $\Delta\Phi/2c$.

[12]We have also studied the signals across a pair of contact points with measuring leads taken toward one side of the circumference when the flux in the sample, which is close to suffering a flux jump, is destroyed by using the strip heater. These results may be more complicated. In particular, the flux density in the sample may not be uniform if the sample has already suffered a flux jump. Essentially similar results are obtained in most of these measurements also. Slight departures which occur in a few cases when the sample has already suffered a flux jump, indicate a partial preferential flux expulsion only through the heated region and may be due to local non uniform flux density in the sample. (See Secs. IV and VI.)

[13]The small signal V_S over a short initial time up to $t \sim 50$ msec from the start in Fig. 6 is due to several practical limitations of our experimental design and may be ignored.

[14]E. W. Urban, NASA Technical Note TN D-6244, 1971 (unpublished), p. 5.

[15]J. Bussiere and M. A. R. LeBlanc, Proceedings Applied Superconductivity Conference, 1972, p. 452 (unpublished).

[16]Since $R_i < R_0$, there may be some asymmetric flux flow from the regions of the wall at a distance from the strip heater (Ref. 6). This may result in slightly greater flux collapse at its inner surface than at the outer surface. Since $R_i \approx R_0$, however, the corresponding correction to the calculated result is expected to be small and is ignored in the present work.

[17]M. S. Walker and J. K. Hulm, Appl. Phys. Lett. 7, 114 (1965).

[18]Y. Iwasa and J. E. C. Williams, J. Appl. Phys. 39, 2547 (1968).

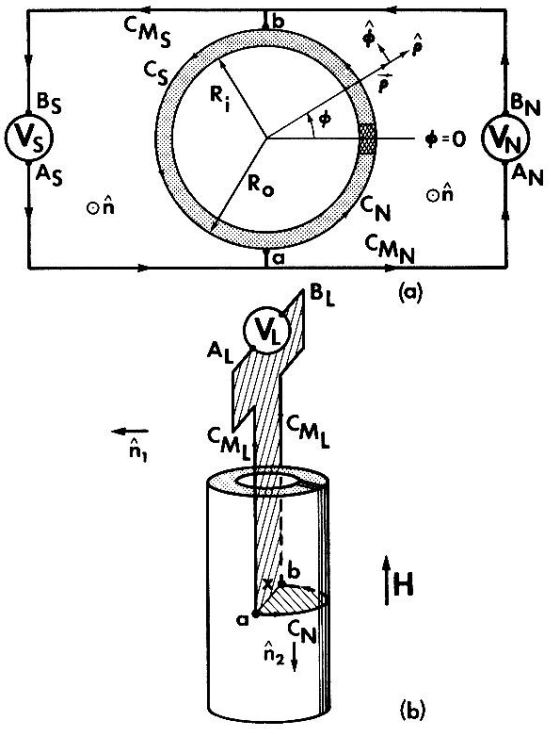

FIG. 10. (a) Schematic of sample cross section and lead arrangements for measurement of voltages V_S and V_N across two contact points a and b on the sample. (See Fig. 3.) The voltage leads are shown some distance from the cylinder only for visual clarity. (b) Configuration of voltage measuring leads when they are taken out along the length of the specimen from the two contact points for measurment of voltage V_L. The area bounded by the measuring leads and the chosen path C_N on the superconductor surface between the contact points is crosshatched. (See Fig. 3.)

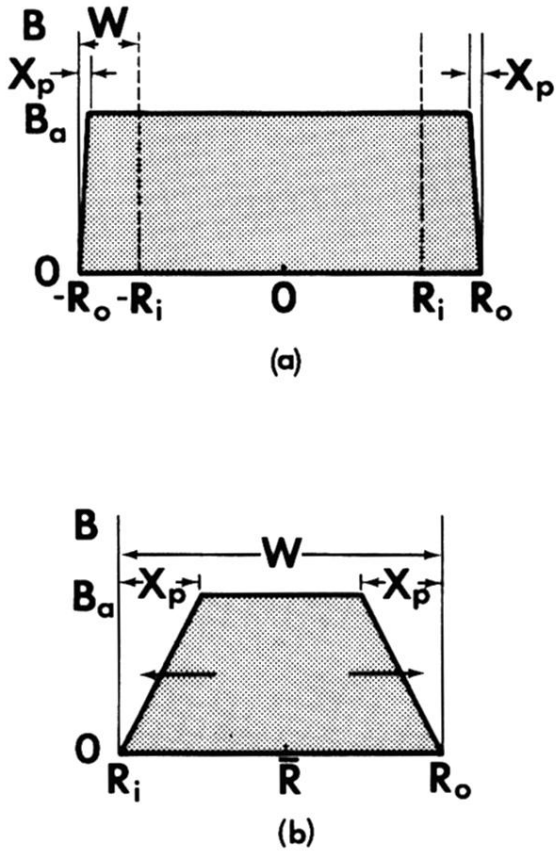

FIG. 11. Sketches of profile of magnetic induction (a) across the cross section of the hollow Nb cylinder trapped initially at $t = t_0$; (b) across the wall of the Nb cylinder after flux from the hole has escaped.

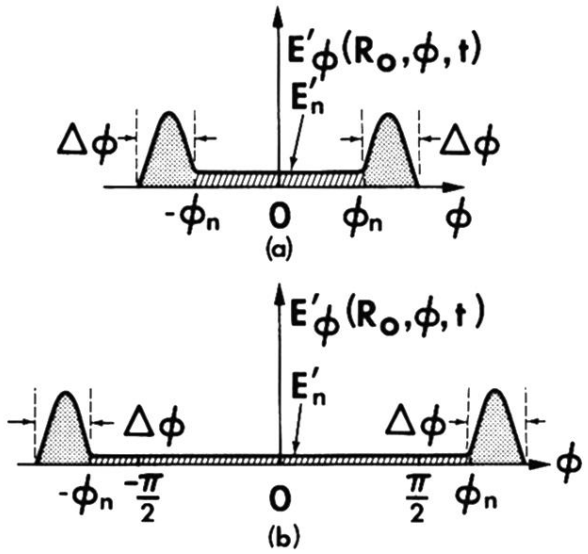

FIG. 13. Sketch of the induced electric field in the normal (crosshatched) and thermal-front (shaded) regions of the cylinder wall (a) during interval II and (b) during interval III. In each case, the total area under the curve in the two humps, corresponding to the thermal fronts, equals the area under the flat portion, corresponding to the heated normal region.

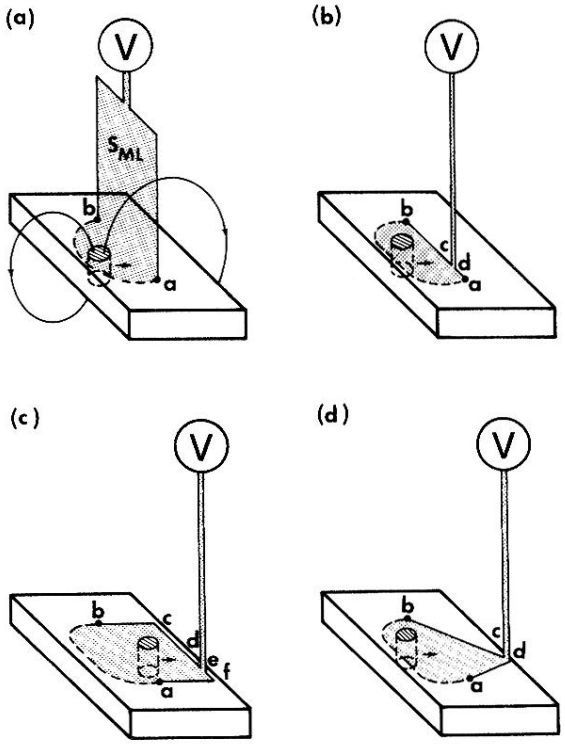

FIG. 2. As described in the text, the flux-flow voltage $V_{ab}(t)$ depends upon the different possible orientations (a), (b), (c), and (d) of the voltage measuring leads relative to the direction of magnetic induction and motion of a vortex line in the superconductor. The time-*integrated* voltage, however, corresponds to the flux in the vortex and is the same in all cases. (The size of the vortex is here greatly exaggerated for clarity.)

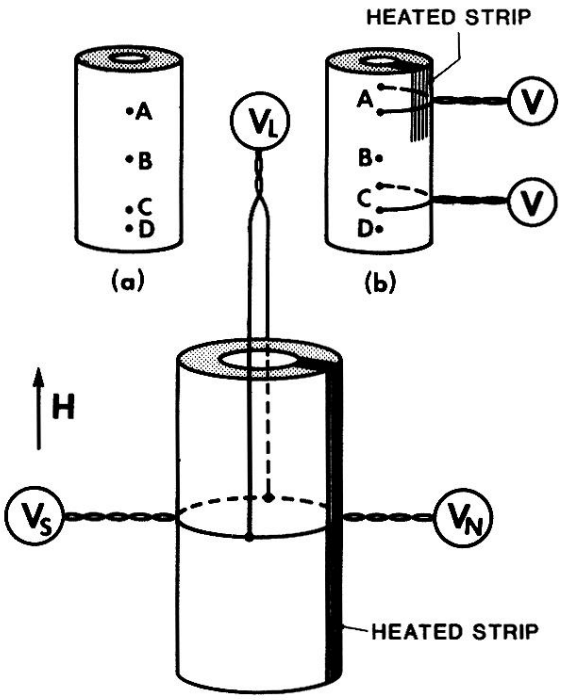

FIG. 3. Schematic view of experimental arrangement. The pick up coils, central heater, and one of the strip heaters are not shown for clarity. Inset (a) shows the location of the pairs of contact points along the length of the cylinder. Inset (b) shows the voltage measuring circuits when a hair-pin heater is used to heat only a part of the length of the specimen.

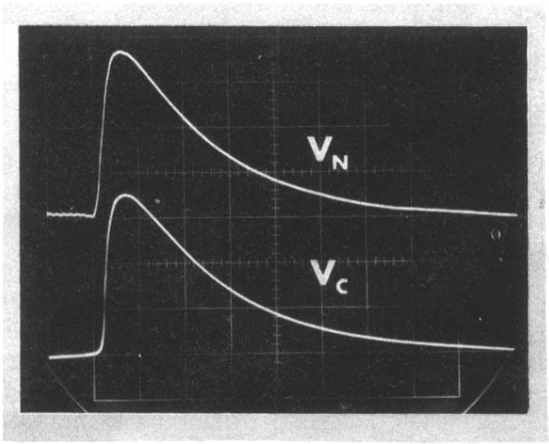

FIG. 4. V_N (upper trace) and V_C (lower trace) during initial stages of collapse of flux mainly from the hole of sample 1. Horizontal scale: 5 msec/division; vertical scale: 2 mV/division; $B_a = 1.594$ kG. See text for explanation of V_N and V_C.

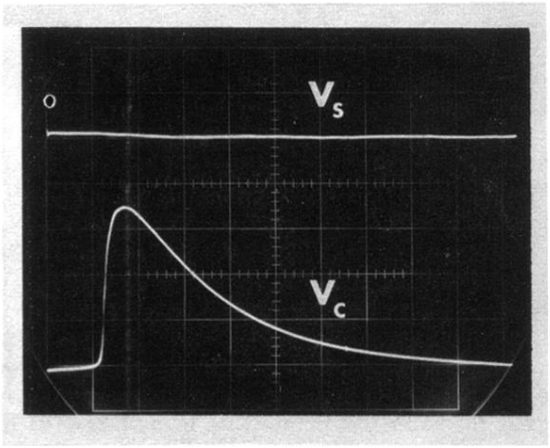

FIG. 5. V_S (upper trace) and V_C (lower trace) during initial stages of collapse of flux mainly from the hole of sample 1. B_a, time sweep and sensitivity as in Fig. 4.

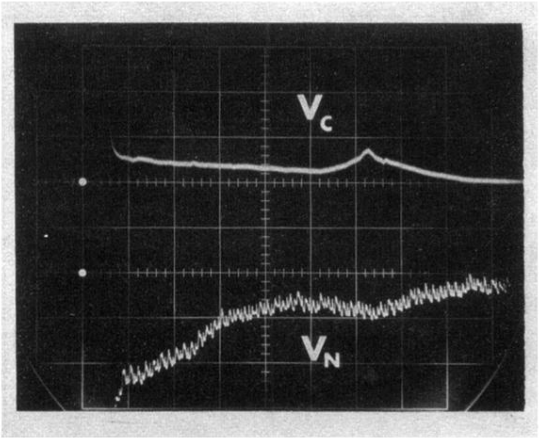

FIG. 6. V_C (upper trace) and $-V_N$ (lower trace) during complete collapse of flux in sample 1. Horizontal scale: 100 msec/division; upper trace: 0.08 mV/division; lower trace: 0.02 mV/division; $B_a = 1.594$ kG. V_C and $-V_N$ during initial stages of flux collapse, shown in Fig. 4, are here off scale.

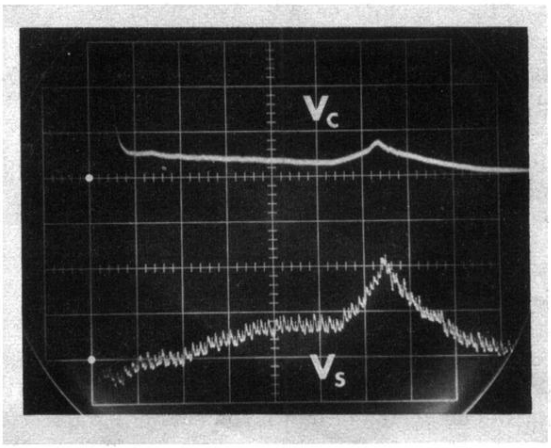

FIG. 7. V_C (upper trace) and V_S (lower trace) during complete collapse of flux in sample 1. B_a, time sweep, and sensitivity as in Fig. 6. V_C during initial stages of flux collapse, shown in Fig. 5, is here off scale.

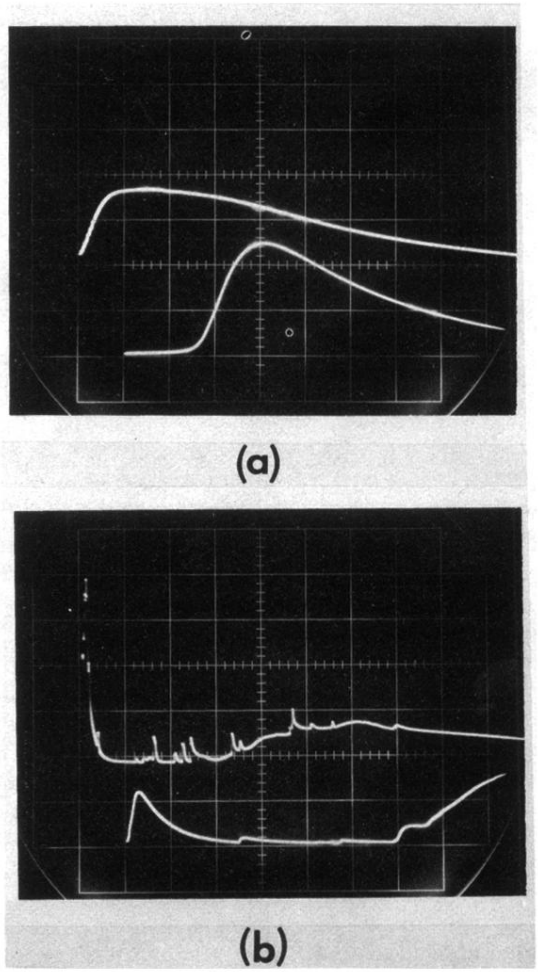

FIG. 9. Instantaneous voltage versus time across identical pick up coils wound around Nb sample 1 at two locations, C (upper trace) and B (lower trace) [see Fig. 3(a)], along its length during spontaneous flux jumps. (a) First flux jump suffered by the virgin sample as the applied magnetic field is increased from zero to 1.945 kG. Horizontal scale: 2msec/division; upper trace = 0,1 V/division; lower trace = 0.1 V/division. (b) The next flux jump as the applied magnetic field is further increased to 3.112 kG. Horizontal scale: 1 msec/division; top trace: 0.2 V/division; lower trace: 0.1 V/division.